AIAA JOURNAL
Vol. 42, No. 4, April 2004

Spectral Element Method for Linear Fan Tone Noise Radiation

D. Stanescu*
McGill University, Montreal, Quebec H3A 2S6, Canada
D. Ait-Ali-Yahia†
Pratt and Whitney Canada, United Technologies Corporation, Longueuil, Quebec J4G 1A1, Canada
W. G. Habashi‡
McGill University, Montreal, Quebec H3A 2S6, Canada
and
M. P. Robichaud§
Pratt and Whitney Canada, United Technologies Corporation, Longueuil, Quebec J4G 1A1, Canada

A numerical method for prediction of acoustic spinning mode radiation from turbofan inlets is presented. Sound propagation is modeled by the linearized mass conservation equation for irrotational flows and solved in the frequency domain. The mean flow through the inlet is obtained as a solution of the full potential equation. Both the mean-flow and the acoustic problem are approximated by Galerkin projection in spectral element spaces of continuous piecewise polynomials defined on the same grid. The Gauss–Chebyshev–Lobatto points within the elements are generated via transfinite interpolation and CAD projection procedures embedded within the code. The linear algebraic systems obtained are then solved using either direct or sparse iterative solvers based on the message passing interface standard for interprocessor communication. The singularity appearing in the acoustic integrals on the symmetry axis is treated by the use of a collocation operator based on the Gauss–Chebyshev, instead of the Gauss–Chebyshev–Lobatto, points. To eliminate reflections from the radiation boundaries, a novel frequency-domain formulation of the matched-layer technique, wherein waves entering the layer are exponentially damped, is proposed. The overall computing procedure is first validated on a tone radiation problem from a semi-infinite cylinder and then applied to an experimental JT15D turbofan inlet setup.

Nomenclature

c	=	speed of sound
$\mathrm{d}s$	=	arclength along $\partial\Omega$
h_j	=	Lagrange interpolant at node j
i	=	$\sqrt{-1}$
J	=	Jacobian matrix
k	=	wave number
M	=	Mach number
$\mathcal{M}$	=	mapping tensor
m	=	azimuthal mode order
N	=	order of Lagrange interpolant
$\boldsymbol{n}$	=	unit normal vector
p	=	pressure
T_p	=	pth-order Chebyshev polynomial
t	=	time variable
$\boldsymbol{V}$	=	velocity vector
(x, r, θ)	=	cylindrical coordinate system
β	=	damping exponent
γ	=	ratio of specific heats
(ξ, η)	=	local coordinate system
ρ	=	density
σ_M	=	damping factor
Φ	=	velocity potential
Ψ	=	weighting function
Ω	=	computational domain
ω	=	reduced frequency

Subscripts

c	=	hard-wall boundary
f	=	inlet boundary
i	=	grid node indices
0	=	mean-flow component
∞	=	far-field boundary
$'$	=	acoustic component

Received 12 July 2002; revision received 10 April 2003; accepted for publication 24 October 2003.

*Research Associate, CFD Laboratory, Department of Mechanical Engineering, 688 Sherbrooke St. West.

†Technical Expert, Department of Multi-Disciplinary Numerical Methods, 1000 Marie-Victorin (01SR4); Djaffar.Ait-Ali-Yahia@pwc.ca. Member AIAA.

‡Professor and Director, CFD Laboratory, Department of Mechanical Engineering, 688 Sherbrooke St. West. Associate Fellow AIAA.

§Manager, Department of Multi-Disciplinary Numerical Methods, 1000 Marie-Victorin (01SR4).

I. Introduction

DESIGNING modern turbofan engines with higher bypass ratios is significantly limited by increasingly restrictive airport noise regulations. Independent of takeoff, cruise, or landing operations, fan rotor-stator interactions remain a major source of engine noise. Interest in modeling, understanding, and reducing this noise has catapulted the relatively recent computational-aeroacoustics (CAA) techniques as major tools in the fan design process.

Pratt and Whitney Canada and McGill University have initiated a joint research effort to develop axisymmetric and three-dimensional nonlinear[1,2] and linear CAA codes for noise radiation from aircraft engines and, more specifically, for fan tone radiation computations. The nonlinear codes, based on the Euler equations with a

multidomain spectral method in space and an explicit $2N$-storage Runge–Kutta in time, were developed to achieve a more complete modeling of sound propagation phenomena. However, for typical industrial applications with high-frequency incoming spinning modes the three-dimensional time-domain codes are still demanding in terms of computer resources and, therefore, are difficult to routinely use in the design process.

A simplified approach based on a linear model of sound propagation, in which the mean-flow computation is decoupled from the acoustic field prediction, has been developed by Roy et al.[3] The methodology involves the solution, in an axisymmetric frame, of the incompressible potential equation for the mean flowfield and a linearized potential equation in the frequency domain for the acoustic field. Both equations are numerically discretized by a Galerkin finite element method, with a direct solution of the resulting linear system of equations. For boundary condition considerations, the mean-flow problem was divided into three subproblems, while wave envelope elements were used in the acoustic problem to reduce reflections at the far field.

Although this approach is attractive for fan noise design purposes, it might eventually become prohibitive for acoustic modes with high frequencies. In fact, an accurate prediction of noise propagation with quadratic isoparametric elements requires a fine mesh spacing, with at least four to five elements (9–11 nodes) per wavelength.[3] The demand on computer resources is further increased by the use of direct solvers. An alternative method based on ray tracing and hence valid in the high-frequencies range was proposed by Dougherty,[4] which neglects flow effects other than some boundary-layer influences.

In the present paper, the linear acoustic model[3] is revisited with several numerical and implementation modifications. The mean-flow solution is upgraded to the full potential equation. This is expected to improve predictions of the radiated sound field because the refraction effects that occur mainly in the region of the inlet aperture are accounted for. Spectral elements based on Chebyshev polynomials are used for the discretization, which brings down the number of necessary points per wavelength to between four and five for a sufficiently large number of Gauss–Chebyshev–Lobatto (GCL) points per element. A modification to the spectral element method is introduced to avoid the singularity on the symmetry axis. The radiation boundary is treated in a novel manner by using a damping layer that preserves phase information within the computational domain proper. The resulting algebraic systems can be solved either by direct or iterative solvers, parallelized to run on distributed memory machines through the use of the PETSc (Portable, Extensible Toolkit for Scientific Computations) library.[5] Finally, GCL grids are systematically generated using a CAD-based approach,[6] embedded within the computer code. These grids can also be dynamically adapted by varying the number of GCL points per element, an input parameter to the code, to yield the minimum number of points per wavelength needed to guarantee a certain level of accuracy.

II. Governing Equations

The equation of mass conservation for irrotational flow can be written as

$$\frac{\partial \rho}{\partial t} + \nabla \cdot (\rho \nabla \Phi) = 0 \tag{1}$$

where the velocity $\boldsymbol{V} = (u, v)$ is related to the potential by $\boldsymbol{V} = \nabla\Phi$. Here, the flow variables are nondimensionalized with respect to the values of the density ρ_∞ and speed of sound c_∞ at the far field, and the fan blade tip radius R is used as a reference length.

Using the isentropic equation of state $p/\rho^\gamma = 1/\gamma$, the momentum equation can be reduced under the irrotationality assumption to an algebraic relation between the density and the velocity potential

$$\rho = \left[1 - (\gamma - 1)\left(\frac{\partial \Phi}{\partial t} + \frac{\nabla\Phi \cdot \nabla\Phi - M_\infty^2}{2}\right)\right]^{1/(\gamma-1)} \tag{2}$$

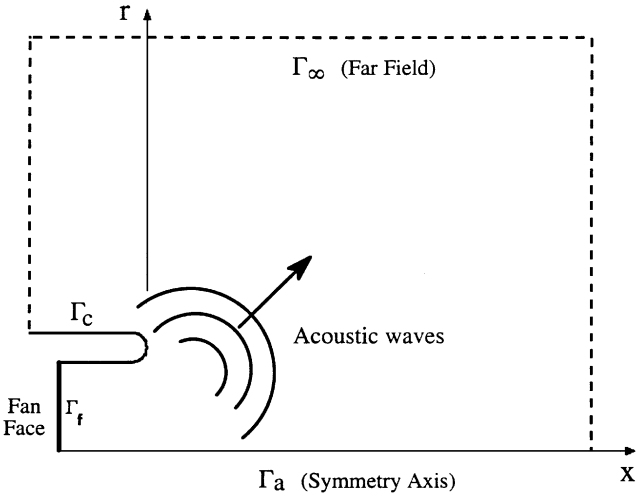

Fig. 1 Typical computational domain.

where the Mach number M_∞ appears on the right-hand side as a result of the specific reference values chosen for nondimensionalization.

The formulation is restricted to turbofan inlets having an axially symmetric geometry. Therefore, a typical domain Ω on which the solution is sought is a part of the (x, r) plane, as shown in Fig. 1. The domain Ω is partitioned into E generalized nonoverlapping quadrilateral elements. The three-dimensional volume generated by the rotation of Ω around the x axis is denoted by $\tilde{\Omega}$. We note that for a function that does not depend on the angular coordinate, namely, $F(x, r, \theta) = f(x, r)$, the volume and surface integrals in three-dimensional space can be expressed as

$$\int_{\tilde{\Omega}} F(x, r, \theta) r \, \mathrm{d}r \, \mathrm{d}x \, \mathrm{d}\theta = 2\pi \int_{\Omega} f(x, r) r \, \mathrm{d}r \, \mathrm{d}x \tag{3a}$$

$$\int_{\partial\tilde{\Omega}} F(x, r, \theta) r \, \mathrm{d}s \, \mathrm{d}\theta = 2\pi \int_{\partial\Omega} f(x, r) r \, \mathrm{d}s \tag{3b}$$

A. Mean-Flow Problem

Consider that the unsteady flowfield results from the superposition of small perturbations, denoted by a prime superscript, over a steady mean flow denoted by subscript 0, such that $\rho = \rho_0 + \rho'$ and $\Phi = \Phi_0 + \Phi'$. The partial differential equation and boundary conditions that determine the mean flow through the inlet can therefore be cast in the following form:

$$\nabla \cdot (\rho_0 \nabla \Phi_0) = 0 \tag{4a}$$

$$\Phi_0 = M_\infty x \qquad \text{on} \qquad \Gamma_\infty \tag{4b}$$

$$\rho_0 \nabla \Phi_0 \cdot \boldsymbol{n} = g \qquad \text{on} \qquad \Gamma_f \tag{4c}$$

$$\nabla \Phi_0 \cdot \boldsymbol{n} = 0 \qquad \text{on} \qquad \Gamma_c \tag{4d}$$

where the mean-flow density is related to the potential by

$$\rho_0 = \left\{1 - [(\gamma - 1)/2]\left(\nabla\Phi_0 \cdot \nabla\Phi_0 - M_\infty^2\right)\right\}^{1/(\gamma-1)} \tag{5}$$

Because Γ_a is not an actual boundary in the three-dimensional space, no boundary condition is required there. This is in fact equivalent to a natural boundary condition on the mean-flow potential, namely, $v_0 = 0$ on Γ_a, once the partial differential equation (4a) is expressed in weak form.

B. Acoustic Problem

The equations governing the perturbations can be obtained by linearization of Eqs. (1) and (2), leading to

$$\frac{\partial \rho'}{\partial t} + \nabla \cdot (\rho_0 \nabla \Phi' + \rho' \nabla \Phi_0) = 0 \tag{6}$$

subject to

$$\rho' = -\frac{\rho_0}{c_0^2}\left[\frac{\partial \Phi'}{\partial t} + \nabla \Phi_0 \cdot \nabla \Phi'\right] \tag{7}$$

For propagation of acoustic waves, the governing equation (6) must be solved subject to a Sommerfeld radiation condition on Γ_∞ and suitable boundary conditions on Γ_f and Γ_c (see Fig. 1). For the purpose of this work, the inlet casing is considered to be a rigid wall. Hence, the boundary condition on Γ_c is zero normal acoustic velocity $\partial \Phi'/\partial n = 0$. It has been customary to suppose that acoustic perturbations reflected by the aperture of the inlet and propagating in the negative x direction are allowed to pass through Γ_f without generating any waves propagating in the positive x direction. Under this approach, the impeding positive-x propagating perturbations are known, and the amplitude of the reflected waves can be computed under the assumption of locally uniform mean flow on Γ_f. For simplicity, the sum of the positive-x and negative-x propagating waves is considered to be known, which corresponds to a Dirichlet boundary condition for the acoustic potential on Γ_f; see Roy et al.[3] for more details.

III. Numerical Approximation

A. Weak Form of the Mean-Flow Problem

The weak formulation of the mean-flow problem is obtained by multiplying the full potential equation (4a) by a suitable test function $\psi_0(x, r)$ and integrating over $\bar{\Omega}$. After taking into account Eqs. (3a) and (3b) and the divergence theorem, one obtains

$$\int_\Omega \rho_0 \nabla \phi_0 \cdot \nabla \psi_0 r \, \mathrm{d}r \, \mathrm{d}x = \int_\Gamma \rho_0 \psi_0 \nabla \phi_0 \cdot \boldsymbol{n} r \, \mathrm{d}s \tag{8}$$

where $\boldsymbol{n}$ is the unit vector normal to the boundary $\Gamma = \Gamma_f \cup \Gamma_\infty \cup \Gamma_c$. Because the mean-flow potential does not depend on the angle θ, the variable $\Phi_0(x, r, \theta)$ has been replaced here by $\phi_0(x, r)$.

Let $N \geq 1$ be a specified integer, and denote by $\mathcal{Q}_N$ the set of real polynomials in the variables x and r such that the degree of any $q \in \mathcal{Q}_N$ in each variable does not exceed N. Note that $\mathcal{Q}_N$ is a real vector space of dimension $(N+1)^2$. Also let $\boldsymbol{X}^E$ be the vector space of real functions continuous on the closure of Ω, whose restrictions to an element are polynomials in $\mathcal{Q}_N$, namely, $\boldsymbol{X}^E = \{f : \bar{\Omega} \to \mathcal{R} : f \in \mathcal{C}^0(\bar{\Omega}), f|_{\Omega_e} \in \mathcal{Q}_N\}$. The trial solution is sought directly in the subset of functions that satisfy the Dirichlet boundary condition on Γ_∞, $\boldsymbol{X}_D^E = \{f \in \boldsymbol{X}^E : f|_{\Gamma_\infty} = M_\infty x\} \subset \boldsymbol{X}^E$. Taking into account the natural boundary condition on Γ_c, the mean-flow problem can be stated in variational form as: find $\phi_0(x, r) \in \boldsymbol{X}_D^E$ such that

$$\int_\Omega \rho_0 \nabla \phi_0 \cdot \nabla \psi_0 r \, \mathrm{d}\Omega = \int_{\Gamma_f} g \psi_0 r \, \mathrm{d}s \tag{9}$$

holds for any $\psi_0(x, r) \in \boldsymbol{X}_{\Gamma_\infty}^E = \{f \in \boldsymbol{X}^E : f|_{\Gamma_\infty} = 0\}$.

An iterative procedure is required to find the solution to the nonlinear equation (9). For example, an application of Newton's method leads to

$$\begin{aligned}
&\int_\Omega \rho_0 \left(1 - \rho_0^{1-\gamma} \boldsymbol{V}_0^2\right) \nabla(\delta\phi_0) \cdot \nabla \psi_0 r \, \mathrm{d}\Omega \\
&\quad - \int_{\Gamma_f} \rho_0 \left(1 - \rho_0^{1-\gamma} \boldsymbol{V}_0^2\right) \nabla(\delta\phi_0) \cdot \boldsymbol{n} \psi_0 r \, \mathrm{d}s \\
&\quad = -\int_\Omega \rho_0 \nabla \phi_0 \cdot \nabla \psi_0 r \, \mathrm{d}\Omega + \int_{\Gamma_f} g \psi_0 r \, \mathrm{d}s
\end{aligned} \tag{10}$$

where $\delta\phi_0$ represents a correction to the velocity potential solution.

B. Weak Form of the Acoustic Problem

Because the spinning modes are periodic both in time and in the circumferential direction,[7] solutions for the acoustic perturbation potential are assumed to take the form $\Phi'(x, r, \theta, t) = \phi(x, r) e^{i(\omega t - m\theta)}$. Here, $\phi(x, r)$ is a complex valued function, the real part of which is the desired solution and $i^2 = -1$.

The weak form of the acoustic problem is obtained by multiplying Eq. (6) by $\Psi(x, r, \theta, t) = \psi(x, r) e^{-i(\omega t - m\theta)}$, consistent with the definition of the inner product in a complex Hilbert space. After the use of the divergence theorem and $\rho'(x, r, \theta, t) = \rho'(x, r) e^{-i(\omega t - m\theta)}$, the acoustic equation becomes

$$\begin{aligned}
&\int_\Omega \psi i\omega\rho' r \, \mathrm{d}\Omega - \int_\Omega \nabla\psi \cdot (\rho_0 \nabla\phi + \rho' \nabla\phi_0) r \, \mathrm{d}\Omega \\
&\quad + \int_{\Gamma_f \cup \Gamma_\infty} \psi (\rho_0 \nabla\phi + \rho' \nabla\phi_0) \cdot \boldsymbol{n} r \, \mathrm{d}s = 0
\end{aligned} \tag{11}$$

Note that all of the quantities under the integrals do not depend on the angle θ but only on m, which is why Eqs. (3a) and (3b) could be used.

To express the contribution on Γ_∞, suppose that this boundary is sufficiently far from the aperture of the inlet so that the noise can be considered as being radiated from a monopole in uniform flow placed at the origin. In this case, the exact form of the acoustic potential is

$$\phi(x, r) = (A/R) e^{i(\omega t - k\Lambda)} \tag{12}$$

where $k = \omega/c_\infty$, $R = \sqrt{[x^2 + (1 - M_\infty^2) r^2]}$, and $\Lambda = (R - M_\infty x)/(1 - M_\infty^2)$. By differentiating Eq. (12), the boundary integrand can be expressed in terms of the acoustic potential[3] as

$$\begin{aligned}
G(\phi) &= (\rho_0 \nabla\phi + \rho' \nabla\phi_0) \cdot \boldsymbol{n} \\
&= [\rho_0 \phi (x n_x + r n_r)/R]\left[-ik - \left(1 - M_\infty^2\right)/R\right]
\end{aligned} \tag{13}$$

It is well known that a prohibitively large computational domain might be needed for this method alone to give good results.

The use of wave elements[3] that incorporate the proper decay of the amplitude with the radius from the source leads to a better approximation of the Sommerfeld boundary condition. However, the construction of such elements usually requires grid lines aligned with the surfaces of constant phase. Moreover, this approach does not necessarily lead to an accurate prediction of the phase of the acoustic pressure.[8]

Recently, an improvement in approximating the nonreflecting boundary condition, based on combining the advantages of the infinite and wave envelope elements, has been proposed by Astley et al.[9] and extended by Eversman[10] to steady uniform flows and turbofan acoustic radiation in a cylindrical coordinate system. This boundary treatment also provides an efficient method for the determination of the far-field acoustic pressure that otherwise would be computed by incorporating a postprocessing procedure such as the Kirchhoff method.[11]

Another alternative for eliminating reflections of waves impinging from the computational domain onto Γ_∞ consists in modifying the governing equation in a relatively small layer of elements next to Γ_∞ by the addition of a damping term

$$\frac{\partial \rho'}{\partial t} + \nabla \cdot (\rho_0 \nabla \Phi' + \rho' \nabla \Phi_0) = -\sigma(\boldsymbol{x}) \rho' \tag{14}$$

where $\boldsymbol{x} = (x, r)$. In this manner, the solution $\rho'(t)$ behaves as the exponentially decaying solution $f = e^{-\sigma t}$ of $\dot{f} = -\sigma f$ for $\sigma > 0$ upon entering the layer.

This approach has already been used successfully in time-domain acoustic computations.[1,12] Its advantages stem from the fact that it is independent of grid topology, is simple to implement, and requires negligible computational overhead. It also allows the exit boundaries to be placed much closer to the noise sources where the flowfield would be highly nonuniform. In this case, a postprocessing

procedure, such as the Kirchhoff method, is required to determine the acoustic solution at the far field.

The quantity $\sigma(\boldsymbol{x})$ is made to vary from 0 at the interior limit of the damping layer to a maximum value on Γ_∞ according to a power law

$$\sigma(\boldsymbol{x}) = \sigma_M \sum_i \left(\frac{x_i - x_i^{\text{int}}}{x_i^{\text{ext}} - x_i^{\text{int}}} \right)^\beta \tag{15}$$

where x_i^{int} and x_i^{ext} are the coordinates of the interior and exterior limits of the absorbing layer, limits that lie along planes on which one coordinate is constant.

Expressing the density from the linearized momentum equation (7), the following variational problem is obtained: find $\phi \in \boldsymbol{Z}_D^E$ such that

$$\int_\Omega \frac{\rho_0}{c_0^2} \Bigg[\left(\omega^2 - \frac{c_0^2 m^2}{r^2} \right) \phi\psi + i\omega u_0 (\phi\psi_x - \psi\phi_x) + i\omega v_0 (\phi\psi_r - \psi\phi_r) + \left(u_0^2 - c_0^2\right)\phi_x\psi_x + \left(v_0^2 - c_0^2\right)\phi_r\psi_r + u_0 v_0 (\phi_x\psi_r + \phi_r\psi_x) - \psi\sigma(i\omega\phi + u_0\phi_x + v_0\phi_r) \Bigg] r \, \mathrm{d}\Omega + \int_{\Gamma_\infty} G(\phi)\psi r \, \mathrm{d}s = 0 \tag{16}$$

holds for any $\psi \in \boldsymbol{Z}_{\Gamma_f}^E$. The complex vector space introduced here is $\boldsymbol{Z}^E = \{f : f = f^R + if^I, f^R, f^I \in \boldsymbol{X}^E\}$. The Dirichlet boundary condition on Γ_f is imposed by considering the trial solution a member of the subset $\boldsymbol{Z}_D^E \subset \boldsymbol{Z}^E$ of functions that satisfy it a priori, and $\boldsymbol{Z}_{\Gamma_f}^E$ is the subspace of functions with zero trace on Γ_f.

C. Spectral Element Discretization

Because the present spectral approximation is based on Chebyshev polynomials, the evaluation of the integrals involved in the weak formulation is carried out on the master element $\Omega_M = [-1, 1]^2$. A one-to-one transformation from Ω_M onto any arbitrary element Ω_e, given by $(x, r) = \mathcal{M}(\xi, \eta)$, is supposed to exist. Such a mapping can be constructed by transfinite interpolation[13] from a description of the edges of the element Ω_e, as further discussed in the following.

The GCL points on the master element correspond to $\xi_i = \eta_i = -\cos(\pi i/N)$ for $i = 0, 1, \ldots, N$. A suitable basis for $\boldsymbol{X}^E$ and $\boldsymbol{Z}^E$ can be constructed from the images of the Lagrange interpolation polynomials based on the points (ξ_i, η_j) through the transformation $\mathcal{M}(\xi, \eta)$. On each element, the trial solution takes the form

$$\phi(x, r) = \sum_{i,j=0}^{N} \phi_{ij} h_i[\xi(x, r)] h_j[\eta(x, r)] \tag{17}$$

where $\phi_{ij} = \phi[\mathcal{M}(\xi_i, \eta_j)]$ denotes either the mean-flow potential or the complex-valued acoustic potential and

$$\sum_{i,j=0}^{N}$$

denotes the double sum

$$\sum_{i=0}^{N} \sum_{j=0}^{N}$$

The $(N+1)^2$ test functions are $\psi_{kl}(x, r) = h_k[\xi(x, r)] h_l[\eta(x, r)]$, where k, l also vary from 0 to N.

The Lagrange interpolants on the master element Ω_M can in turn be conveniently expressed[14] in terms of the Chebyshev polynomials $T_p(x) = \cos[p \arccos(x)]$ caused by the particular position of the points ξ_i:

$$h_i(\xi) = \prod_{p \neq i}^{N} \left(\frac{\xi - \xi_p}{\xi_i - \xi_p} \right) = \frac{2}{N c_i} \sum_{p=0}^{N} \frac{T_p(\xi_i) T_p(\xi)}{c_p} \tag{18}$$

with $c_i = 2$ if $i = 0$ or $i = N$ and $c_i = 1$ otherwise.

For the test function ψ_{kl}, the volume integrals in (x, r) space can be recast as volume integrals over the master element, that is,

$$I_{kl} = \int_{-1}^{1} \int_{-1}^{1} \mathcal{L}_\phi \phi(\xi, \eta) \mathcal{L}_\psi \psi_{kl}(\xi, \eta) f(\xi, \eta) \, \mathrm{d}\xi \, \mathrm{d}\eta \tag{19}$$

where the operator $\mathcal{L} \in \{1, \partial/\partial\xi, \partial/\partial\eta\}$. The function $f(\xi, \eta)$ contains a product of terms related to the mean flow, the Jacobian of the transformation $J = |\partial(x, r)/\partial(\xi, \eta)|$, the corresponding metric terms, and the radius r.

To evaluate the integral, the function $f(x, r)$ is replaced by its spectral interpolant

$$f(x, r) = \sum_{m,n=0}^{N} f[\mathcal{M}(\xi_m, \eta_n)] h_m(\xi) h_n(\eta) \tag{20}$$

so that the integral becomes

$$I_{kl} = \sum_{i,j=0}^{N} S_{klij} \phi_{ij} \tag{21a}$$

where

$$S_{klij} = \sum_{m,n=0}^{N} f_{mn} \int_{-1}^{1} \mathcal{L}_\phi^i h_i(\xi) \mathcal{L}_\psi^k h_k(\xi) h_m(\xi) \, \mathrm{d}\xi \times \int_{-1}^{1} \mathcal{L}_\phi^j h_j(\eta) \mathcal{L}_\psi^l h_l(\eta) h_n(\eta) \, \mathrm{d}\eta \tag{21b}$$

The operators acting on the Lagrange interpolants are such that for example $\mathcal{L}_\phi^i = \partial/\partial\xi$ if $\mathcal{L}_\phi = \partial/\partial\xi$ and unity otherwise. The integrals on the right-hand side can now be evaluated by replacing the interpolants by their expression (18) and directly computing the integrals of products of Chebyshev polynomials. An example of such a computation with $\mathcal{L}_\phi = \mathcal{L}_\psi = 1$ is given by Korczak and Patera.[15] Note that, although two indices are used for the nodal values of ϕ, which is natural because of the tensor product form of the trial solution, the expression (21a) represents the formation of (a part of) the element stiffness matrix S. Furthermore, quantities of the form

$$\int_{-1}^{1} \mathcal{L}_\phi^i h_i(\xi) \mathcal{L}_\psi^k h_k(\xi) h_m(\xi) \, \mathrm{d}\xi$$

are computed once and stored at the beginning of the computation.

A complication arises for elements having one edge on the axis of symmetry Γ_a because for nodes on such an edge the radial coordinate is $r = 0$, and the integrand in Eq. (15) becomes singular.

One alternative to eliminate this singularity, while keeping the same accuracy, consists of modifying the present spectral element method for the axial elements only. The collocation interpolant for $f(x, r)$ based on the GCL points is replaced by the interpolant based on the Gauss–Chebyshev (GC) points $\bar{\xi}_m = \bar{\eta}_m = -\cos[(m - \frac{1}{2})\pi/N]$ for $m = 1, 2, \ldots, N$ such that

$$f(x, r) = \sum_{m,n=1}^{N} \bar{f}_{mn} \bar{h}_m(\xi) \bar{h}_n(\eta)$$

where $\bar{f}_{mn} = f[\mathcal{M}(\bar{\xi}_m, \bar{\eta}_n)]$ and the new Lagrange interpolants are given by

$$\bar{h}_m(\xi) = \prod_{p \neq m}^{N} \left(\frac{\xi - \bar{\xi}_p}{\bar{\xi}_m - \bar{\xi}_p} \right) = \frac{2}{N} \sum_{p=0}^{N-1} \frac{T_p(\bar{\xi}_m) T_p(\xi)}{c_p} \tag{22}$$

Formation of the elemental matrix is now accomplished in a manner similar to Eq. (21a) and involves integrals of the form

$$\int_{-1}^{1} \mathcal{L}_\phi^i h_i(\xi) \mathcal{L}_\psi^k h_k(\xi) \bar{h}_m(\xi) \, \mathrm{d}\xi$$

which are also calculated and stored in the same manner. Data used in the evaluation of $\tilde{f}_{mn}$ can be computed by interpolating from the corresponding data at the GCL points, at the price of a matrix-vector multiplication.[1,16]

D. Linear Solvers

The system of equations resulting from the mean-flow problem has a symmetric and positive definite matrix and can be solved very efficiently by conjugate gradient iteration. On the other hand, the complex matrix obtained from the discretization of the acoustic problem must be solved with a direct solver or with an iterative method valid for general matrices. The use of an iterative solver, which only requires storage of the nonzero entries of the matrix, is always desirable if a sufficiently fast converging method can be found. To experiment with a wide range of iterative solvers designed for use on parallel distributed memory machines, while keeping the possibility to use direct solvers, the PETSc library[5] has been used. This library offers a collection of data structures at a high level of abstraction, which greatly facilitates the task of solving partial differential equations in a parallel environment. Under this approach the code for matrix assembly is the same for both direct and iterative solvers, and different solvers and preconditioners can be chosen at run time as a command line option.

IV. Grid Generation

Unlike finite difference or finite element methods, spectral element methods use grids that are composed of nonoverlapping elements discretized into a set of GCL points. These grids should not only respect the GCL point distribution in all spatial directions but also conserve the integrity of the boundary curves. These two properties prevent the straightforward use of standard commercial grid-generation codes, unless one has access to their projection libraries and CAD files.

The present aeroacoustic code is enhanced with a GCL grid-generator module,[6] which makes use of the ICEM-CFD Hexa module. First, the CAD file is read within the ICEM-CFD software and then subdivided into a set of coarse elements to produce a background grid. The resulting background grid is read in a typical finite element format within the aeroacoustic code, wherein a data structure is built for the internal and boundary nodes. The required number of GCL points per element is first evaluated based on the reduced frequency, a characteristic element edge length, and the number of required GCL points per wavelength. An unprojected spectral element grid is then generated by first discretizing the grid edges to GCL points and then constructing the grid within the element by a two-dimensional transfinite interpolation procedure. Finally, the spectral element grid is constructed by projecting the GCL boundary points on the CAD curves using ICEM-CFD projection libraries.

This grid generation procedure is compatible with several CAD system formats, such as CATIA and ICEM-DDN, and allows arbitrary geometries with complex topology to be represented with high fidelity. It can also be viewed as a p-adaptive method wherein the number of GCL points, which represents the order of Lagrange interpolation functions, could be adjusted by the user or in an automatic way, to yield the minimum number of points per wavelength in all space directions needed to guarantee a certain level of accuracy of the numerical solution. Furthermore, it frees the acoustic designer from setting up a new grid for each incoming acoustic mode, thus rendering fan noise analysis for multiple harmonics of blade passage frequency (BPF) a practical undertaking.

V. Results and Discussion

A. Semi-Infinite Cylinder

The first test concerns the radiation of sound from a semi-infinite cylinder of zero wall thickness without a mean flow. Radiation of both plane wave and first radial modes are considered in the axisymmetric case $m = 0$, with a reduced frequency $\omega = 10.3$. The computational domain extends nine length units from the duct exit in the axial direction and the same distance from the axis in the radial direction. This domain is partitioned into 162 elements, on which a number of GC points between $N = 6$ and 8 have been used, corresponding to a number of points per wavelength (PPW) approximately between 4 and 4.9. It was found that for PPW $= 4$ the acoustic field is slightly underresolved; therefore, subsequent numerical experiments have been performed with PPW $= 5$.

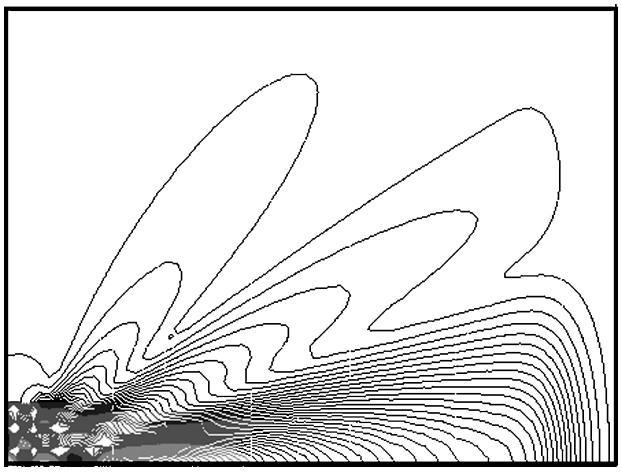

Fig. 2 Contours of acoustic pressure for plane wave mode radiation from a circular cylinder.

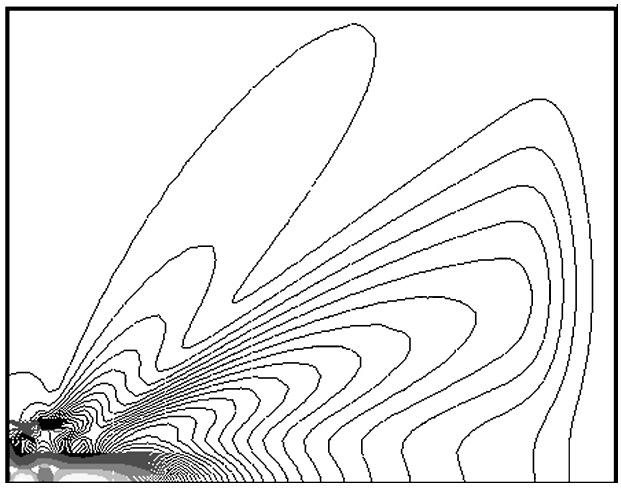

Fig. 3 Contours of acoustic pressure for first radial mode radiation from a circular cylinder.

Figures 2 and 3 display contours of acoustic pressure for both plane wave and first radial modes, respectively. Both solutions were obtained with a number of GC points of $N = 8$.

Figures 4 and 5 compare sound-pressure-level (SPL) directivities with an analytical solution for radiation from a plane circular piston, vibrating in the same mode, as obtained by Tyler and Sofrin.[7] The agreement between the computation and the analytical solution is excellent except at very high angles. This is to be expected because at these values the influence of the walls, for which the analytical solution does not account for, becomes more important.

The performance of Krylov subspace iterative solvers and different preconditioning techniques has been assessed on this problem. This study was performed for $N = 8$, which leads to a linear complex system of 10,660 equations with 1,004,000 nonzero coefficients. Figure 6 shows that an incomplete lower–upper (LU) factorization with a zero level of fill-in, ILU(0), is a sufficient preconditioner to converge all considered Krylov subspace methods. The convergence of QMR and BiCGSTAB solvers requires nearly half of GMRES iterations and twice more CPU time per iteration, which makes all solvers equal in terms of efficiency.

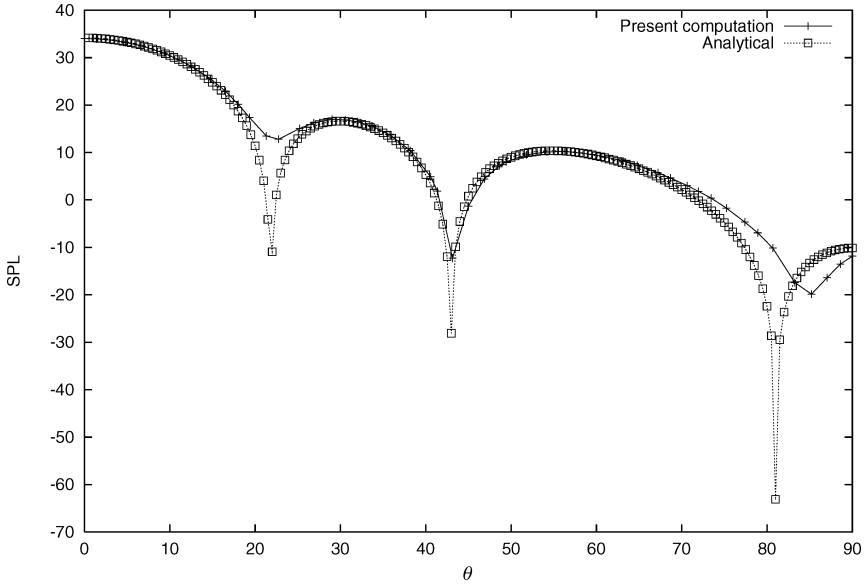

Fig. 4 SPL directivity for plane wave radiation from a circular cylinder.

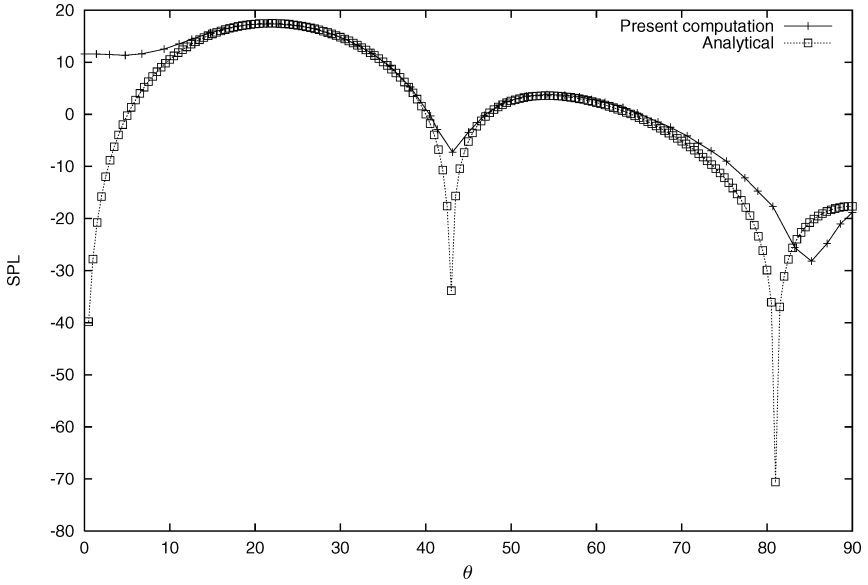

Fig. 5 SPL directivity for first radial mode radiation from a circular cylinder.

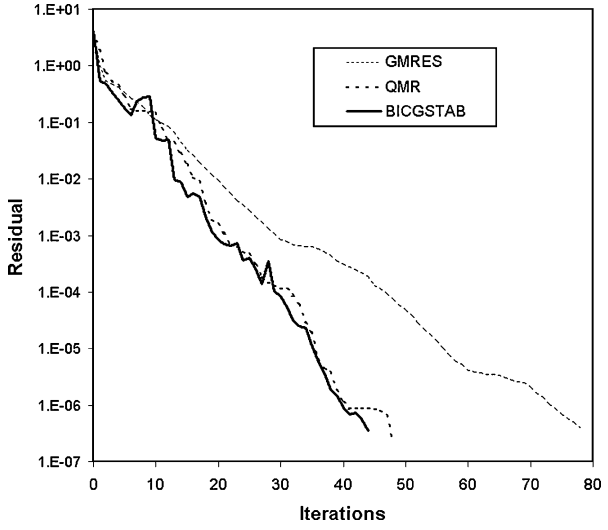

Fig. 6 Comparison between GMRES, QMR, and BICGSTAB convergence plots for the circular cylinder.

The effect of number of GC points on GMRES convergence with ILU(0) preconditioner is also investigated. Three progressive meshes with 6, 8, and 9 GC points per edge are considered. This provides increasing larger system of 6040, 10,660, and 13,450 equations, respectively. Figure 7 demonstrates the efficiency of the GMRES solver because doubling the total number of equations increases the number of iterations by less than 50%.

B. Performance of Boundary Conditions

Treating the fan inlet as a simple source radiating in an uniform flowfield can lead to very large reflections from the far-field boundary. In particular, we noticed in our computations that the part of the boundary Γ_∞ that is closest to the nacelle, that is, on the left-hand side in Fig. 1, cannot usually be placed sufficiently far from the aperture of the nacelle for the simple source assumption to be a reasonable approximation. This boundary can lead to large spurious reflections, responsible for the creation of an interference pattern and a corresponding increase in the acoustic energy present in the computational domain.

However, the use of the damping layer allowed us, in all of the numerical experiments performed, to obtain a solution virtually free

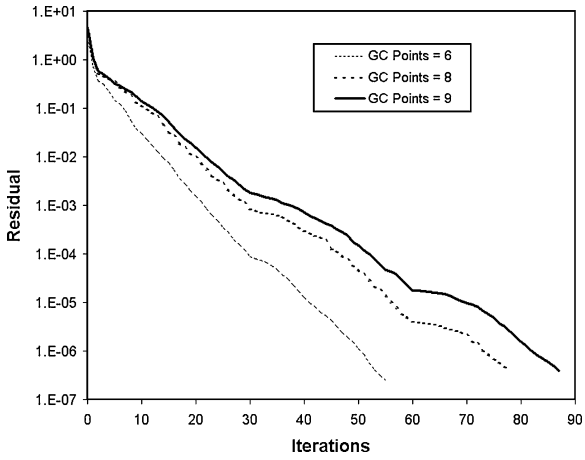

Fig. 7 Convergence of GMRES iterative solver for the circular cylinder with different number of Gauss–Chebyshev points.

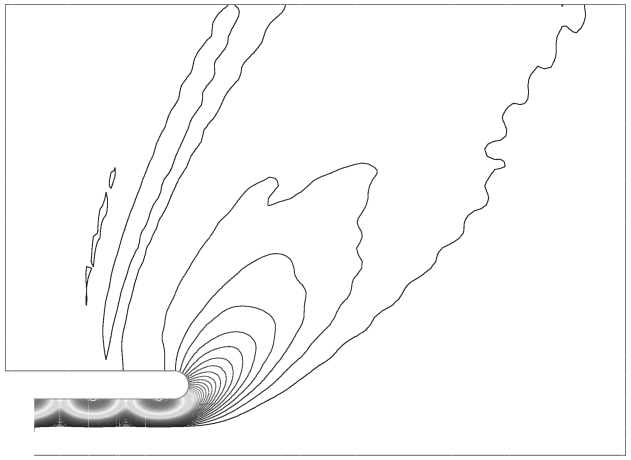

Fig. 8 RMS pressure contours for the bell-mouth inlet, (6, 0) mode, using the monopole radiation boundary condition without a damping layer.

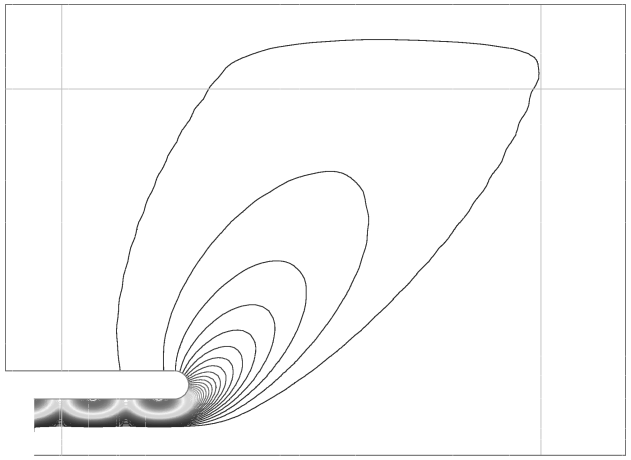

Fig. 9 RMS pressure contours for the bell-mouth inlet, (6, 0) mode, using the monopole radiation boundary condition with a damping layer.

of spurious reflections. To show the effectiveness of this approach, results are presented here for the propagation of the first radial mode $(m, 0)$, in the absence of a mean flow, from two configurations, a bell-mouth inlet with $m = 6$ and $\omega = 8$ and a generic flight turbofan inlet with $m = 0$ and $\omega = 24.4$.

In the bell-mouth case, the computational domain extends about 10 wavelengths from the aperture of the inlet, in both the axial and radial direction, and is partitioned into 105 elements with $N = 10$.

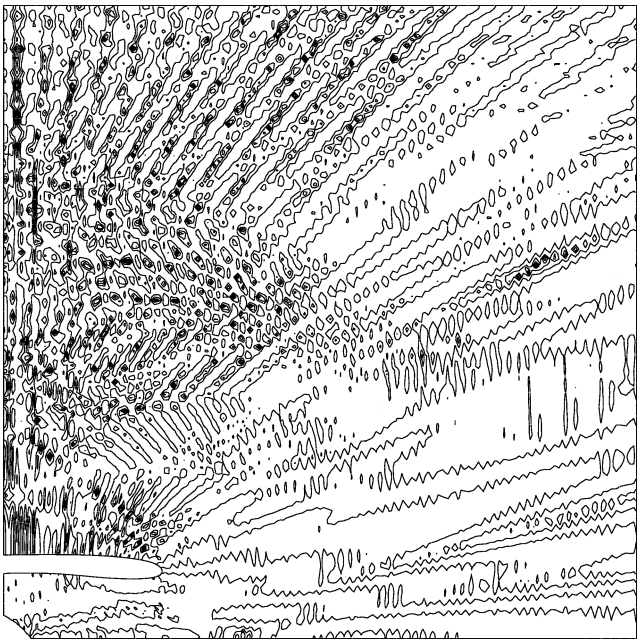

Fig. 10 SPL contours for a generic flight inlet, (0, 0) mode, using the monopole radiation boundary condition without a damping layer.

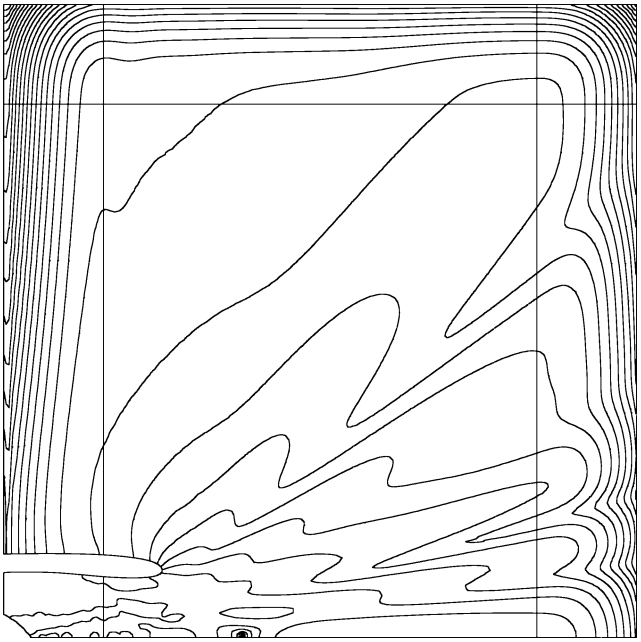

Fig. 11 SPL contours for a generic flight inlet, (0, 0) mode, using the monopole radiation boundary condition with a damping layer.

For the generic flight inlet, the computational domain is made up of 314 elements and $N = 10$ and extends about 40 wavelengths in both directions from the source position. In both cases, the number of points per wavelength is kept above PPW = 5.

Contours of the acoustic pressure amplitude for the first case are presented in Figs. 8 and 9. In this case the monopole boundary condition behaves reasonably well, but it is obvious that the use of the damping layer further improves the quality of the solution. The second case deviates more from the simple source assumption, and the solution displayed in Fig. 10 without a damping layer is practically useless. The introduction of a damping layer allows a clear identification of all the radiated lobes, as can be seen in Fig. 11. Notice also that the SPL contours remain perfectly continuous across the interface with the layer.

C. JT15D Inlet

Measurements of the noise radiated from a modified JT15D engine inlet in flight have been presented by Preisser et al.[17] An array of 41 small diameter rods has been installed on the casing of the nacelle, such that their interaction with the 28 fan blades generated modes with circumferential order $m = 13$ turning at the BPF. Computations have been performed for a range of engine fan speeds, and results are presented for two fan settings corresponding to 8010 and 10,460 rpm, respectively. In both cases, a mesh with $E = 1616$ elements has been used, with the number of GCL points selected such that the number of points per wavelength is at least five. Figure 12 shows this mesh in the region of the inlet.

In the first case, all circumferential modes equal or below $m = 13$ are cut on. The current analysis is, however, limited to the interaction mode (13, 0). Boundary conditions have been specified in terms of the mass flow rate at the fan face, set to 16.6 kg/s, and the far-field Mach number $M_\infty = 0.204$.

The mean-flow solution was computed using Newton's method. At each iteration, the approximate solution of the linearized problem was obtained by conjugate gradient iteration with diagonal preconditioning. Figure 13 shows the convergence in the L_2 norm of the residual in Newton's method for this case for two different number of iterations of the conjugate gradient solver. The linear system arising from the acoustic problem could be solved iteratively but with an ILU(1) preconditioner. The mean-flow Mach number contours are given in Fig. 14, and the computed directivity is compared with the experimental data in Fig. 15.

For the second fan setting, corresponding to 10,460 rpm, the radial mode (13, 1) can also propagate through the inlet and to the far field. In this the relative amplitude and phase of the propagating modes is not known, and so mode (13, 1) was arbitrarily considered to have a very small amplitude compared to the first mode. It is thus hoped to obtain a relatively good description of the principal radiation lobe, despite loosing some accuracy for high values of the directivity angle θ. In addition, for this case, Preisser et al.[17] present results for a static test in which a slightly modified inlet geometry has been tested on a stand, with flow only through the inlet. The boundary conditions used to simulate the mean flow correspond to a mass flux rate of 21.3 kg/s, with $M_\infty = 0$ in the static case and $M_\infty = 0.192$ in the case with forward flight. Figure 16 shows the result for the directivity in the far field. The results successfully predict the main tendency of the radiated field, but it is obvious that not all of the

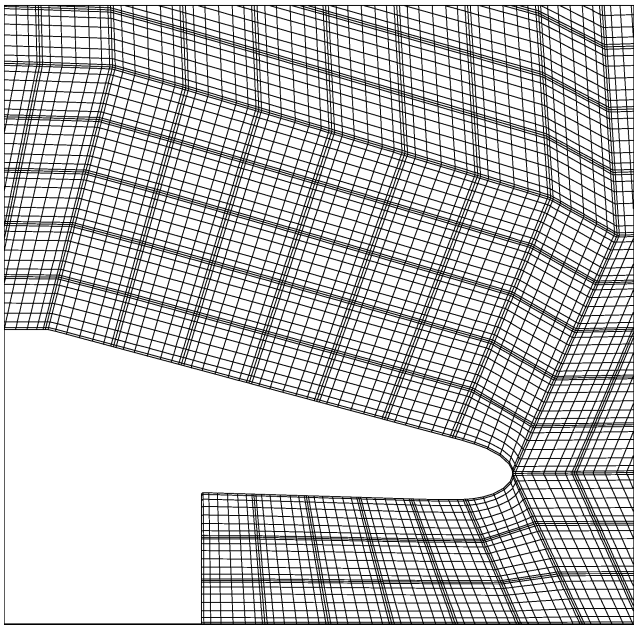

Fig. 12 Mesh in the inlet region for the JT15D engine.

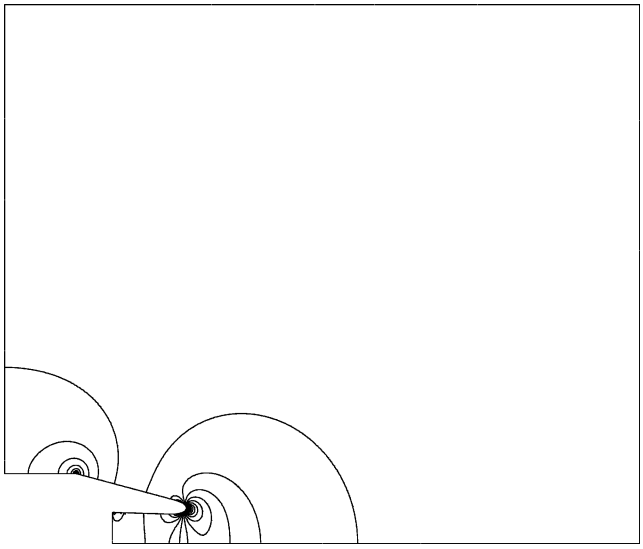

Fig. 14 Mach-number contours for the mean flow through the JT15D engine at 8010 rpm.

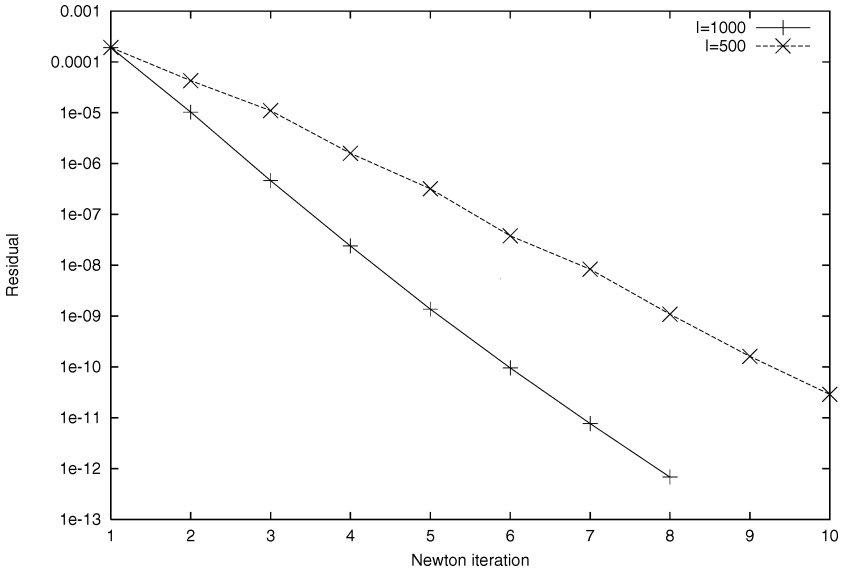

Fig. 13 Convergence of Newton's method for the mean-flow problem, for different numbers of iterations of the conjugate gradient solver.

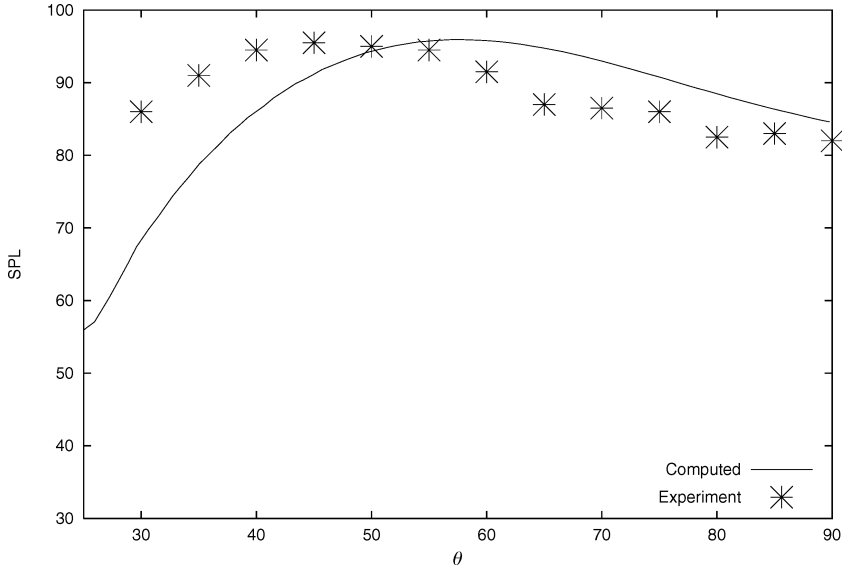

Fig. 15 SPL directivity, JT15D at 8010 rpm.

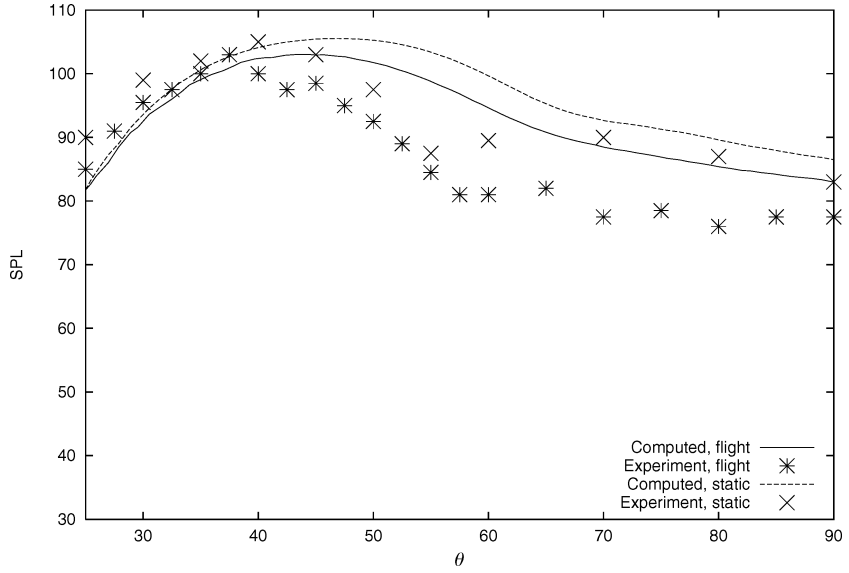

Fig. 16 SPL directivity, JT15D at 10,460 rpm.

factors that influence radiation from the inlet are accounted for in the linearized irrotational flow model.

VI. Conclusions

A spectral element method has been developed for computational modeling of spinning mode radiation from turbofan inlets. The method incorporates an automatic spectral grid generator that uses CAD geometry files to project discretization points on the inlet surface. A radiation boundary condition in the frequency domain has been developed and shown to be effective in eliminating unwanted reflections from the far–field boundary. The iterative solution of both mean-flow and acoustic systems of equations was efficiently achieved through the use of PETSc library. The present methodology was validated on both analytical and experimental test cases. The results demonstrate the ability of the current approach to resolve relevant acoustic phenomena with half of the grid points needed by other similar solvers.

References

[1]Stanescu, D., Ait-Ali-Yahia, D., Habashi, W. G., and Robichaud, M., "Multidomain Spectral Computations of Sound Radiation from Ducted Fans," *AIAA Journal*, Vol. 37, No. 3, 1999, pp. 296–302.

[2]Ait-Ali-Yahia, D., Stanescu, D., Robichaud, M., and Habashi, W. G., "Spectral Element Grid Generation and Nonlinear Computations for Noise Radiation from Aircraft Engines," AIAA Paper 99-1832, May 1999.

[3]Roy, I. D., Eversman, W., and Meyer, H. D., "Improved Finite Element Modeling of the Turbofan Engine Inlet Radiation Problem," NASA Rept., Contract NAS3-25952, April 1993.

[4]Dougherty, R. P., "Nacelle Acoustic Design by Ray Tracing in Three Dimensions," AIAA Paper 96-1773, May 1996.

[5]Balay, S., Gropp, W. D., McInnes, L. C., and Smith, B. F., "PETSc User Manual," Argonne National Lab., ANL-95/11, Rev. 2.0.24, 1999.

[6]Ait-Ali-Yahia, D., Stanescu, D., Robichaud, M., and Habashi, W. G., "Three-Dimensional Spectral Element Grid Generator" (submitted for publication).

[7]Tyler, J. M., and Sofrin, T. G., "Axial Flow Compressor Noise Studies," *SAE Transactions*, Vol. 70, 1962, pp. 309–332.

[8]Rumsey, C. L., Biedron, R. T., Farassat, F., and Spence, P. L., "Ducted-Fan Engine Acoustic Predictions Using a Navier–Stokes Code," *Journal of Sound and Vibration*, Vol. 213, 1998, pp. 643–664.

[9]Astley, R. J., Coyette, J.-P., and Cremers, L., "Three Dimensional Wave Envelopes Elements of Variable Order for Acoustic Radiation and Scattering. Part I. Formulation in the Frequency Domain," *Journal of the Acoustical Society of America*, Vol. 103, 1998, pp. 49–63.

[10]Eversman, W., "A Reflection Free Boundary Condition for Propagation in Uniform Flow Using Mapped Infinite Wave Envelope Elements," *Journal of Computational Acoustics*, Vol. 8, 2000, pp. 25–41.

[11]Roy, I. D., and Eversman, W., "Far-Field Calculations for Turbofan Noise," *AIAA Journal*, Vol. 39, No. 12, 2001, pp. 2255–2261.
[12]Yang, B., Gottlieb, D., and Hesthaven, J. S., "Spectral Simulation of Electromagnetic Wave Scattering," *Journal of Computational Physics*, Vol. 134, 1997, pp. 216–230.
[13]Hesthaven, J. S., "A Stable Penalty Method for the Compressible Navier–Stokes Equations. III. Multi Dimensional Domain Decomposition Schemes," *SIAM Journal on Scientific Computing*, Vol. 20, No. 1, 1999, pp. 62–93.
[14]Patera, A. T., "A Spectral Element Method for Fluid Dynamics: Laminar Flow in a Channel Expansion," *Journal of Computational Physics*, Vol. 54, No. 3, 1984, pp. 468–488.
[15]Korczak, K. Z., and Patera, A. T., "An Isoparametric Spectral Element Method for Solution of the Navier–Stokes Equations in Complex Geometry," *Journal of Computational Physics*, Vol. 62, No. 2, 1986, pp. 361–382.
[16]Kopriva, D. A., and Kolias, J. H., "A Conservative Staggered-Grid Chebyshev Multidomain Method for Compressible Flows," *Journal of Computational Physics*, Vol. 125, No. 1, 1996, pp. 244–261.
[17]Preisser, J. S., Silcox, R. J., Eversman, W., and Parrett, A. V., "A Flight Study of Tone Radiation Patterns Generated by Inlet Rods in a Small Turbofan Engine," AIAA Paper 84-0499, Jan. 1984.

H. M. Atassi
Associate Editor